J. Fluid Mech. (1995), *vol.* 291, *pp.* 323–341

Dissipation and ordering in capillary waves at high aspect ratios

By BO CHRISTIANSEN†, PREBEN ALSTRØM AND MOGENS T. LEVINSEN

Center for Chaos and Turbulence Studies, Niels Bohr Institute, Ørsted Laboratory, DK-2100 Copenhagen Ø, Denmark

(Received 5 November 1993 and in revised form 12 December 1994)

We present an experimental study of high-aspect-ratio Faraday waves. We have measured the dispersion relation and the damping rate, together with the critical amplitude for the primary instability for a wide range of frequencies. We find that our results are well explained by the linear theory, if damping from the moving contact line is considered in addition to the bulk damping. Just above the primary instability a seemingly disordered stationary state is observed. We argue that this state is a superposition of normal modes. Approximately 5% above the primary instability this state breaks down in favour of a quasi-crystalline state. This result is discussed, partly in the light of the recent third-order nonlinear theory.

1. Introduction

The Faraday experiment, i.e. the generation of surface waves on a fluid subjected to purely vertical vibrations, has a long and interesting history. Much of the current interest in the Faraday experiment is due to its possibilities as a system with many degrees of freedom and especially as a pattern forming system. For this purpose the Faraday experiment has two main advantages: the aspect ratio (container size/wavelength) can be varied simply by varying the frequency, and the dynamics can be investigated visually. A surprising result for high aspect ratios is the observation that the relief of the surface may take the form of ordered patterns closely resembling two-dimensional crystals. However, the real surprise is that these patterns are not limited to cells of a particular geometry. For high aspect ratios the boundaries become less important and the geometry is that of the infinite plane. This had been noticed by Faraday (see Martin 1932). Further detailed studies were carried out by Lord Rayleigh (1883) who observed the formation of a square surface pattern. A century later the square pattern was reported and studied for a circular geometry by Ezerskii, Korotin & Rabinovich (1985) and Ezerskii *et al.* (1986). In the same year Aleksandrov *et al.* (1986) found a hexagonal pattern for amplitudes of the drive below those for which they observed the square pattern. A similar pattern had already been reported by Faraday (1831, §93). Pattern selection for intermediate aspect ratios has been investigated by Douady & Fauve (1988) and Douady, Fauve & Thual (1989). Recently, observations of quasi-crystalline patterns have attracted much attention (Christiansen, Alstrøm & Levinsen 1992; Edwards & Fauve 1993). These patterns are macroscopic continuous analogues of molecular quasi-crystals: they possess long-range order and have a forbidden rotational symmetry.

The theoretical basis of the pattern formation is not yet fully understood, although

† Present address: Danish Meteorological Institute, DK-2100 Copenhagen Ø, Denmark.

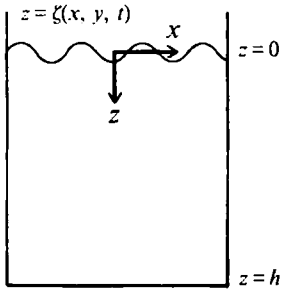

FIGURE 1. The experiment and the comoving reference system.

a few attempts have been made (Ezerskii *et al.* 1986; Levin & Trubnikov 1986; Milner 1991). However, damping rates seem to play a crucial role in the selection of the surface pattern. Experimental work in this direction has almost exclusively dealt with the bounded system (Henderson 1990, 1991), and only sporadic data exist for the extended system (see the discussion in Milner 1991). In this paper we present a study of the dispersion relation, the damping rates and the primary threshold for high aspect ratios in a circular system.

The rest of the paper is organized as follows. In §2 we present the theory. In §3 the experimental set-up is described and the results for the dispersion relation, the damping rate, and the primary threshold are presented. The normal modes and the transition to the quasi-crystalline state is discussed in §4. We close the paper in §5 with a conclusion.

2. Theory

2.1. *The ideal fluid*

The experimental situation is easily described in words: a cell filled with a fluid to a depth h is oscillated vertically with amplitude f and frequency 2ω. To give a mathematical description it is convenient to choose a reference system at rest relative to the cell. The origin of the vertical z-axis is chosen so that the unperturbed surface is given by $z = 0$ and the positive direction is downward. The situation is sketched in figure 1.

As noted by Faraday and later confirmed by Lord Rayleigh the frequency of the excited surface waves is half of the forcing frequency. The subharmonic nature of the instability was theoretically verified directly from the hydrodynamics by Benjamin & Ursell (1954). For later use we outline the linear theory following Meron & Procaccia (1986).

If the viscosity is ignored the hydrodynamical equations can be written in terms of the velocity potential ϕ and the surface deviation ζ. For an incompressible fluid the Laplace equation is fulfilled in the bulk,

$$\nabla^2\phi = 0. \tag{1}$$

Furthermore the fluid satisfies two equations on the surface $z = \zeta$. The first is the Bernoulli theorem (an integral of the Navier–Stokes equation)

$$\partial\phi/\partial t + \tfrac{1}{2}(\nabla\phi)^2 = -p/\rho + [g - \bar{f}\cos(2\omega t)]\,z, \tag{2}$$

where

$$p = \alpha\nabla\cdot\frac{\nabla\zeta}{[1+(\nabla\zeta)^2]^{1/2}}, \tag{3}$$

ρ is the density, g is the gravitation constant, $\bar{f} = 4\omega^2 f$ is the amplitude of the acceleration, and α is the surface-tension coefficient. The second equation is the

kinematic surface condition, expressing that no fluid enters or leaves the surface (Lamb 1963),

$$\frac{\partial \zeta}{\partial t}+\frac{\partial \zeta}{\partial x}\frac{\partial \phi}{\partial x}+\frac{\partial \zeta}{\partial y}\frac{\partial \phi}{\partial y}-\frac{\partial \phi}{\partial z}=0. \tag{4}$$

These equations must be completed with a set of appropriate boundary conditions on the walls and the bottom. The validity of the potential flow approximation will be discussed later.

Linearizing the above set of equations for a lateral unbounded system of finite depth h, and seeking solutions in the form of plane waves,

$$\zeta = a(t)\exp(\mathrm{i}\boldsymbol{k}\cdot\boldsymbol{x}), \tag{5}$$

and

$$\phi = b(t)\exp(\mathrm{i}\boldsymbol{k}\cdot\boldsymbol{x})\,F(z), \tag{6}$$

the system reduces to Mathieu's equation

$$\ddot{a} = -\omega^2[p-2q\cos(2\omega t)]\,a. \tag{7}$$

The constants are given by

$$p=\omega_k^2/\omega^2, \quad q=kf\tanh kh/(2\omega^2), \tag{8}$$

and the dispersion relation is

$$\omega_k^2 = gk(1+\lambda_*^2 k^2)\tanh kh. \tag{9}$$

Here k is the magnitude of the wave vector $\boldsymbol{k}$. The material constant $\lambda_* = (\alpha/g\rho)^{1/2}$ is called the capillary length.

In order to consider the stability of the flat surface one has to study the asymptotic solution of the damped Mathieu's equation. Fortunately the stability criterion for Mathieu's equation is well known. For a comprehensive treatment see e.g. Jordan & Smith (1977). It turns out that two series of resonances exist with frequency ω_k equal to 2ω and ω, respectively. The dominant resonances are subharmonic, with V-shaped borders given by $p = 1 \pm q$. In $(\omega,\bar{f})$-space the subharmonic tongues are parabolic with minimum $\bar{f}=0$ for $\omega=\omega_k$. The tongues of the other resonances are more narrow. Thus, for the unbounded system, where there is no constraint on ω_k, the flat surface becomes unstable when f exceeds the threshold $f_c = 0$.

The case considered above is that of a lateral unbounded system, where the normal modes can be chosen as plane waves. Under this assumption the wavenumber k and therefore the frequency ω_k and p (for a given ω) can be chosen from the continuum. If the system is bounded the wavenumber is limited to a discrete set of values and for a given ω the minimum for q may not be realized. In this case the instability curve consists of pieces of the V-shaped tongues. If the aspect ratio of the system is increased the distance between the tongues will decrease and for high aspect ratios the instability threshold $f_c = 0$ is recovered.

For a circular geometry the normal modes are $J_l(k_{lm}r)\cos(l\theta)$, where J_l are the Bessel functions of order l. The wavenumbers are determined by the boundary condition, i.e. k_{lm} is the mth zero of $(\mathrm{d}J/\mathrm{d}r)(k_{lm}R)$, where R is the radius of the cell. The physical meanings of l and m are the number of angular maxima and the number of nodal circles, respectively.

2.2. *Including damping*

Up to now the effect of damping has not been considered in the discussion. The amplitude a of free surface waves decays as a result of viscous damping, $a \sim \exp(-\gamma t)$, where the damping constant γ is defined in terms of the dissipation of mechanical energy, $\overline{\dot{E}_{mech}/E_{mech}} = -2\gamma$. In addition to the viscous damping in the bulk (Landau & Lifshitz 1987)

$$\gamma_{bulk} = 2\nu k^2, \tag{10}$$

where ν is the kinematic viscosity, several other mechanisms contribute to the damping constant γ. These contributions originate from the thin boundary layers near the fixed walls, the moving contact line, and the free surface if contaminated. We now briefly consider these effects in turn.

On the fixed boundaries the no-slip condition must apply for the viscous fluid. This means that the velocity components parallel to the boundary must change from the finite value given by the inviscid theory to zero over the short distance of order $\delta = (\nu/2\omega)^{1/2}$. This gives rise to big velocity gradients of order δ^{-1} as the normal component of the velocity is zero in the boundary layer (Landau & Lifshitz 1987). As the volume of the boundary layer is proportional to δ and therefore small, it is the effect of the huge velocity gradients that makes the dissipation non-negligible. A straightforward calculation gives (Milner 1991)

$$\gamma_{wall} = \omega\delta/L, \tag{11}$$

where L is the linear size of the cell.

On the free surface the velocity again has to adjust from the value given by the inviscid theory to the demands of the viscous theory over the distance δ. But in this case the no-slip condition does not apply, hence the velocity gradients do not have to be big. Therefore, as the volume is small, the dissipation of energy in the boundary near the free surface can be ignored. Contamination with surface-active molecules may alter this conclusion dramatically. The finite compressibility increases the dissipation of energy in the boundary layer. This problem has been thoroughly studied by Miles (1967). In the limiting case of an incompressible surface layer the surface acts as a fixed wall and Milner (1991) finds

$$\gamma_{surf} = \omega\delta k, \tag{12}$$

as an estimate of magnitude. The exact value depends on the bulk modulus of the surface layer in a complicated way.

A moving contact line is only possible if the no-slip condition is violated. This violation takes place on a microscale s that depends both on the length of the fluid molecules and on the surface roughness. Computing the work done by the surface tension as the contact angle changes and the contact line moves, Milner (1991) finds

$$\gamma_l = \frac{8\omega \ln(R/s)\, k\delta^2 \sin\theta_0}{L(\theta_0 - \sin\theta_0 \cos\theta_0)}, \tag{13}$$

where θ_0 is the static contact angle and R is the macroscopic length at which the surface is no longer flat. Milner suggests the estimates $s = 10$ Å, $R = \delta$, and $\theta_0 = \pi/2$. Note that γ_l is not very sensitive to the exact value of s. The above expression is a maximum value as contact-line hysteresis has not been considered.

In §3.3 we show how the experimentally obtained damping rates can be explained by considering only bulk damping γ_{bulk} and contact-line damping γ_l. The contact line damping gives a noticeable contribution for drive frequencies up to 150 Hz, corresponding to aspect ratios as high as 25. The damping γ_{wall} from the lateral walls turns out to be an order of magnitude smaller. The estimate γ_{surf} of the damping from a contaminated surface typically exceeds the bulk damping by a factor of 4. However, we observe no signature of contamination in our experiment.

To implement the damping, the term $-2\gamma\dot{a}$ is added on the right-hand side of (7). In the presence of damping the previous V-shaped borders of the dominant subharmonic tongues become hyperbolic

$$p = 1 \pm [q^2 - (2\gamma/\omega)^2]^{1/2}. \tag{14}$$

For $p = 1$ the minimum value $q_c^1 = 2\gamma/\omega$ for q is obtained. The minima of the other narrow resonances are larger than q_c^1. This explains why the isochronous instability is

not found in experiments: for lower drive amplitude the flat surface has already become unstable to oscillations with half the drive frequency (Meron & Procaccia 1986; Douady 1990). Inserting q from (8) into $q_c^1 = 2\gamma/\omega$ gives the threshold for the unbounded system $\bar{f}_c = 4\omega\gamma/(k \tanh kh)$ or

$$f_c = \gamma/(k\omega \tanh kh). \tag{15}$$

If the system is bounded the instability curve consists of pieces of the hyperbolic tongues.

2.3. *Nonlinear theory*

As we have seen the flat surface becomes unstable at a critical amplitude f_c of the external drive. Just above f_c, normal modes are excited. However, the normal-mode range decreases with increasing aspect ratio, approaching zero for an infinite system. In such an extended system with no lateral boundaries the neutral modes are plane waves with the magnitude of the wave vector given by the dispersion relation. Thus, on the instability threshold an infinity of modes are already free to be excited. These modes lie on the circle in $\boldsymbol{k}$-space. Increasing the drive amplitude above f_c turns the neutral circle in $\boldsymbol{k}$-space into an unstable band. If the band is narrow, as it will be close to f_c, the effect can be described as a small variation on top of the neutral modes, i.e. the plane waves will be modulated by an amplitude slowly varying in space and time.

To describe the spatial structure of the surface state the linear theory does not suffice, as pattern selection is a nonlinear effect. Recently, a few attempts to develop a nonlinear theory have been performed (Levin & Trubnikov 1986; Milner 1991). In this section we briefly review Milner's work and discuss its limitations.

Assuming a surface state composed of standing waves we seek solutions of the form (Milner 1991)

$$\zeta = \sum_j a_j(x,t) \exp \mathrm{i}(\boldsymbol{k}_j \cdot \boldsymbol{x} - \omega t) + \text{c.c.}, \tag{16}$$

$$\phi = -\frac{\mathrm{i}\omega}{k} \exp kz \sum_j a_j(x,t) \exp \mathrm{i}(\boldsymbol{k}_j \cdot \boldsymbol{x} - \omega t) + \text{c.c.} \tag{17}$$

Notice that the above expressions are chosen to be solutions of the linearized equations if the amplitudes $a_j(x,t)$ are constants. Exploiting the three basic symmetries of the system: invariance under a translation in time and invariance under translation and rotation in space, the general form of the amplitude equations is found. It can be shown that only standing waves are excited. Up to third order and omitting gradient terms, the amplitude equations for the standing wave amplitudes A_j have the form (Malomed, Nepomnyashchii & Tribelskii 1989)

$$\frac{\partial A_j}{\partial t} = \gamma\epsilon A_j - \sum_l \Gamma(\Theta_{lj}) A_l^2 A_j. \tag{18}$$

Here ϵ is the forcing $\epsilon = (f - f_c)/f_c$, and Θ_{lj} is the angle spanned by $\boldsymbol{k}_l$ and $\boldsymbol{k}_j$. The coupling function $\Gamma(\Theta)$ obeys the symmetries $\Gamma(\Theta) = \Gamma(\pi - \Theta)$ and $\Gamma(\Theta) = \Gamma(-\Theta)$, and combinatorical arguments enforce the discontinuity $\Gamma(0) = \Gamma(\Theta \to 0)/2$ (Malomed *et al.* 1989; Müller 1993; Cross & Hohenberg 1993).

The above equation is derivable from the Luapunov functional

$$F = -\tfrac{1}{2}\gamma\epsilon \sum_l A_l^2 + \tfrac{1}{4} \sum_j \sum_l \Gamma(\Theta_{jl}) A_j^2 A_l^2. \tag{19}$$

Under the assumption of a regular pattern with amplitudes $A_j = A$ consisting of N wave vectors equidistantly distributed on the half-circle, F attains its minimum $-(\gamma\epsilon)^2 N/(4\sum_{l=1}^{N} \Gamma(\Theta_{jl}))$ for $A^2 = \gamma\epsilon/\sum_{l=1}^{N} \Gamma(\Theta_{jl})$. The most stable pattern is obtained

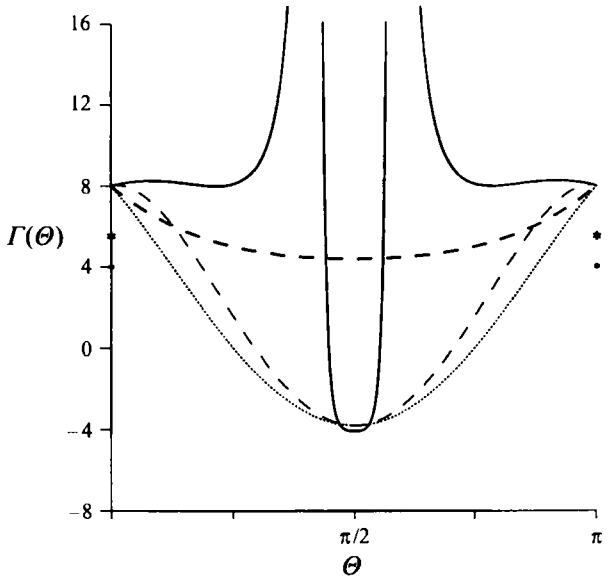

FIGURE 2. The function $\Gamma(\Theta)$ (in units of νk^4) obtained by Milner (1991) (solid curve). The three other functions are fourth-order polynomials heuristically constructed to fulfil the stability criteria for rolls (thick dashed curve), squares (thin dashed curve), and an octagonal quasi-crystal (dotted curve), respectively. The dot (·) and the star (*) at $\theta = 0$, π indicate the two values $\Gamma(\theta \to 0)/2$ and $2\nu k^4 + \Gamma(\theta \to 0)/2$ (Milner 1991) used for $\Gamma(0)$ ($= \Gamma(\pi)$).

by minimizing $\bar{\Gamma}(N) = (1/N)\sum_{l=1}^{N} \Gamma(\Theta_{jl})$ with respect to N. Thus, either rolls ($N = 1$), squares ($N = 2$), hexagons ($N = 3$), or octagonal quasi-crystals ($N = 4$) are favoured depending on the relative values of $\bar{\Gamma}(1) = \Gamma(0)$, $\bar{\Gamma}(2) = [\Gamma(0) + \Gamma(\pi/2)]/2$, $\bar{\Gamma}(3) = [\Gamma(0) + 2\Gamma(\pi/3)]/3$, and $\bar{\Gamma}(4) = [\Gamma(0) + 2\Gamma(\pi/4) + \Gamma(\pi/2)]/4$. For example, the octagonal quasi-crystalline pattern is more stable than the square pattern when $\bar{\Gamma}(4) < \bar{\Gamma}(2)$, i.e. when $\Gamma(\pi/4) < [\Gamma(0) + \Gamma(\pi/2)]/2$. In general, the more flat $\Gamma(\Theta)$ is around $\pi/2$ (assuming $\Gamma(\pi/2) < \Gamma(0)$), the higher the values of N that are favoured. As illustrative examples we show in figure 2 three different coupling functions $\Gamma(\Theta)$, heuristically constructed to support rolls, squares, and octagonal quasi-crystalline patterns, respectively. Each of the patterns is stable in a finite region of phase-space. See Malomed *et al.* (1989) for more details on the conditions for stability for both regular and non-regular stationary states.

To find the specific form of the coupling function $\Gamma(\Theta)$, Milner applies the method of multiple scales (Newell & Whitehead 1969). The result is shown in figure 2. We find $\bar{\Gamma}(1) = 4.00\nu k^4$, $\bar{\Gamma}(2) = -0.04\nu k^4$, $\bar{\Gamma}(3) = 8.76\nu k^4$, and $\bar{\Gamma}(4) = 4.03\nu k^4$. The small negative value of $\bar{\Gamma}$ for $N = 2$ indicates the presence of a slight subcriticality (Milner uses $\Gamma(0) = 2\nu k^4 + \Gamma(\Theta \to 0)/2$, which increases the values of $\bar{\Gamma}(N)$ by $(2/N)\nu k^4$, thereby finding the square pattern to be the most favoured). However, figure 2 is strongly dominated by a divergence at $\Theta = \cos^{-1}(2^{1/3} - 1) \sim 74.9°$ (and at the symmetrical value $\theta = 180° - 74.9°$). The divergence originates from the omission of higher harmonics in the expansions (16) and (17). One may speculate that the inclusion of such terms will change the above results for $\bar{\Gamma}(N)$.

Much more serious are the limitations enforced by neglecting fifth-order (and maybe higher-order) terms in the amplitude equations (for the square pattern fifth-order terms must necessarily be considered). To estimate the value of ϵ at which fifth-order terms become important, we use Milner's expression for the sixth-order functional under the

assumption of a regular pattern of N modes (all $A_j = A$), and the assumption of a small 'detuning' $\sigma = \Delta\omega(k)$ (expressed as a frequency by (9)) compared to γ,

$$F = -\tfrac{1}{2}\gamma\epsilon NA^2 + \tfrac{1}{4}N^2\bar{\Gamma}(N)A^4 + (1/48\gamma)N^3\bar{T}(N)^2A^6. \tag{20}$$

The fifth-order coupling function $\bar{T}$ is derived in Milner (1991). The optimum amplitude A corresponding to F being at its minimum is given by

$$A^2 = \frac{-\bar{\Gamma}(N) + [\bar{\Gamma}(N)^2 + \tfrac{1}{2}\epsilon\bar{T}(N)^2]^{1/2}}{N\bar{T}(N)^2/4\gamma}. \tag{21}$$

For $\epsilon \to 0$, we retrieve the old result $A^2 = \gamma\epsilon/N\bar{\Gamma}(N)$. From (21) it is clear that the fifth-order term becomes important at $\epsilon = \epsilon_c \approx \bar{\Gamma}(N)^2/\bar{T}(N)^2$. This value of ϵ turns out to be extremely small. While $\bar{\Gamma}(N) \approx \nu k^4$, $\bar{T}(N) \approx \omega k^2$; thus $\epsilon_c \approx (\nu k^2/\omega)^2$. For a typical frequency of $\omega/\pi = 380$ Hz in our ethanol-based experiment, we find $\epsilon_c \approx 3 \times 10^{-4}$, which is one order of magnitude below our forcing accuracy, and two orders of magnitude below the width of our normal-mode range, above which we first observe a stable pattern. Obviously, the third-order nonlinear theory is not well-suited for low-viscosity experiments.

At higher viscosities (or in general at higher damping rates), the third-order theory is more appropriate. The analysis above suggests studies at $\gamma/\omega \sim 0.1$. Such high-aspect-ratio experiments have, however, not yet been carried out. The damping must not be too high, however, since detuning then becomes important, moving the divergences closer to $\Theta = \pi/2$. Such a detuning has a substantial effect on $\bar{\Gamma}(3)$ and $\bar{\Gamma}(4)$, which decrease rapidly with detuning. The value of $\bar{\Gamma}(1)$ remains essentially unchanged, while the theoretical subcriticality for the square pattern may increase slightly. At a detuning of 5° we estimate the $\bar{\Gamma}$ values to be (from Milner 1991, figure 1) $\bar{\Gamma}(1) \sim 4\nu k^4$, $\bar{\Gamma}(2) \sim -\nu k^4$, $\bar{\Gamma}(3) \sim 5.5\nu k^4$, and $\bar{\Gamma}(4) \sim 2.5\nu k^4$. At a larger detuning (viscosity), the value of $\Gamma(\pi/2)$ increases rapidly, eventually leading to a substantial increase of $\bar{\Gamma}(2)$ and $\bar{\Gamma}(4)$.

3. Experiments

3.1. *The experimental set-up*

In this section we describe our experimental set-up for the study of Faraday waves. A cylindrical cell was fastened to a 13 cm high rack firmly connected to a Brüel & Kjær vibration exciter type 4809. This was driven by a programmable Stanford Research Systems synthesized function generator DS 345, which was controlled by a personal computer. The shaker itself rested on a huge stone disk (60 cm in diameter, 10 cm thick) supported by three rubber feet to eliminate vibrations from the surroundings. Figure 3 shows a schematic drawing of the set-up, which resembles that of Ciliberto & Gollub (1984, 1985). The aim of the rack is to allow a mirror to be placed below the cell. The mirror forms an angle of 45° with the horizontal plane and makes it possible to project light through the cell.

The dimensions of the cell in most experiments were 8.4 cm in interior diameter and 2 cm in height. The cell was made by attaching a thin ring of glass or Plexiglas to a circular glass plate. The cell was closed by a 0.2 cm thick matt glass plate, which served three purposes: it kept the fluid from being polluted, it minimized the evaporation, and it scattered the light for an image to form. In this image wave maxima appear as bright regions because the concave surface focus the projected light. Correspondingly, wave minima appear as dark regions.

The fluid used in the experiments was ethanol or propanol alcohol. The cell was filled

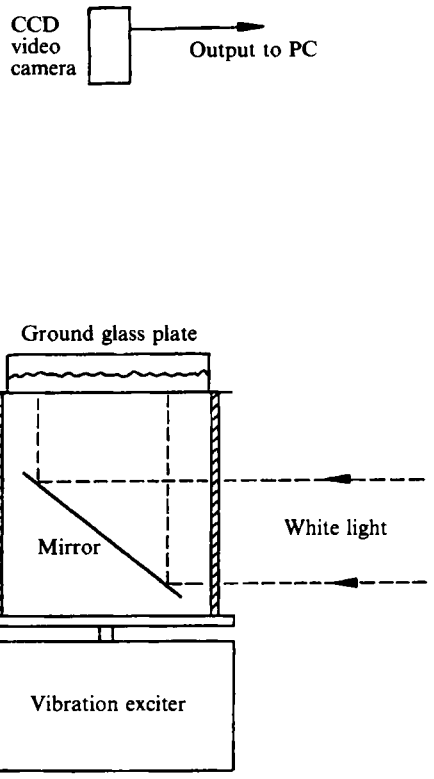

FIGURE 3. Schematic drawing of the experimental set-up.

to a depth of 1–1.5 cm. This depth is much larger than the wavelength of the surface waves for the interval of frequencies 50–500 Hz that we consider. At 400 Hz, the wavelength is 1.7 mm. The upper limit is given by the maximum acceleration, $\sim 10g$, of the shaker. This acceleration depends on the payload which in our experiment is approximately 300 g. For frequencies above 500 Hz the acceleration required for the first instability is larger than the maximum acceleration of the shaker. Below 50 Hz surface waves emitted from the boundaries are visible. These waves are generated by the meniscus and fall off rapidly into the cell (Douady 1990), with a penetration length that decreases with increasing frequency. They differ from the subharmonic Faraday waves by being synchronous with the drive. The contribution to dissipation from the moving contact line (cf. (13)) is discussed further in §3.3.

A Brüel & Kjær MM 0002 magnetic transducer was positioned 2–10 mm above a disk of high permeability fastened to either the cell or the rack. The output of this device is a current proportional to the instantaneous velocity of the disk. The sensitivity is essentially independent of the frequency up to 2000 Hz, according to specifications. The current was amplified with an EG & G preamplifier model 113 and digitized on a Data Precision 6000A wave analyser. To measure the amplitude of the surface waves a photo diode was placed slightly above the matt glass plate, and the signal was amplified with a preamplifier and sent to the Data 6000A wave analyser, where it was digitized. The diode is not subject to the vibrations, which suggests that a correction needs to be made for the relative motion. However, this was not found necessary as the signal was almost zero for drive amplitudes less than the critical amplitude, i.e. for the unperturbed surface. The Data 6000A wave analyser was connected to a personal computer, where the data were sent for further analysis.

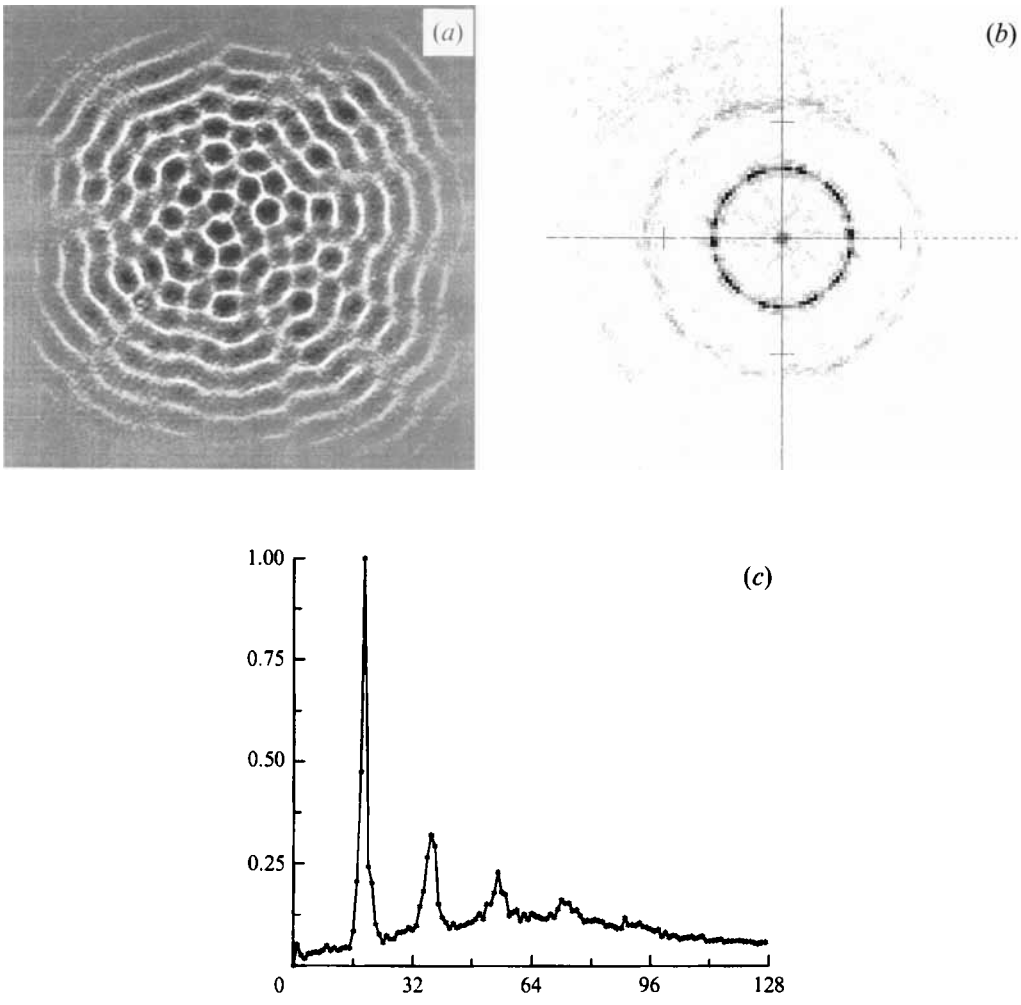

FIGURE 4. (*a*) The digitized image after applying a 25% square window. (*b*) Spatial Fourier spectrum of the image in (*b*). (*c*) The logarithm of the radial spectrum as function of the wavenumber k (arbitrary units).

Efforts were made to keep the cell horizontal. We found the best way was to excite the circular waves found for drive amplitudes just above the critical. We then adjusted the set-up until the pattern was centred and stationary. Even with the best of efforts it was impossible to avoid a slow overall drift of the pattern. The amplitude of the drift is approximately 0.1 mm s^{-1}.

3.2. *The dispersion relation*

We have measured the dispersion relation in the frequency range 50–500 Hz. For fixed frequency we adjust the amplitude to be in the interval slightly above f_c, where stable circular patterns are found. With the camera in a position where most of the cell is visible an image is acquired. Inhomogeneities in the illumination are removed by dividing point by point with a background image of the unperturbed surface. The resulting picture is then Fourier transformed with an FFT routine. The spectrum consists of a set of concentric rings representing the basic wavelength and its

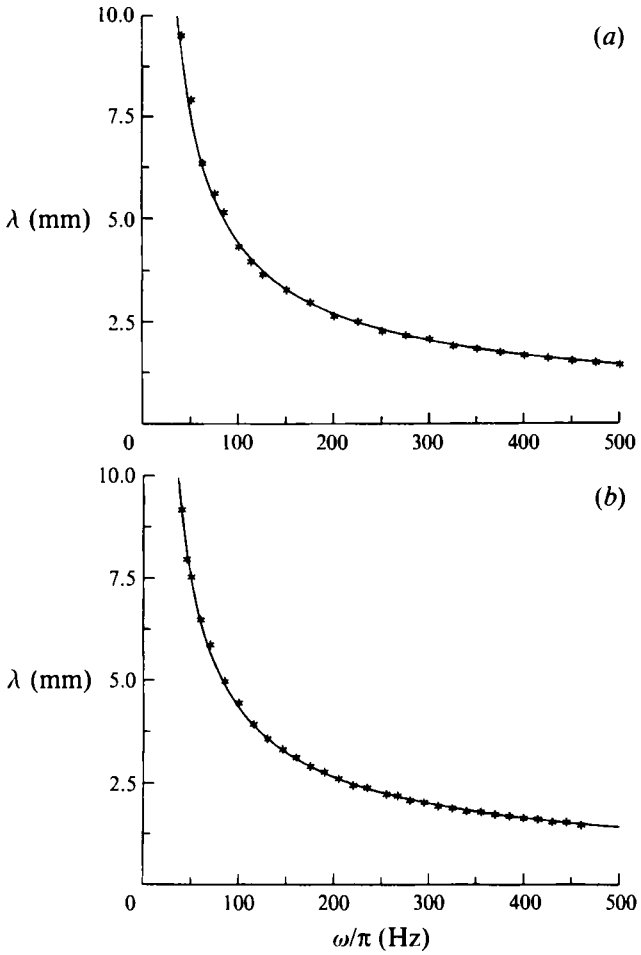

FIGURE 5. The wavelength λ (in mm) as a function of the drive frequency ω/π, where (*a*) the fluid is ethanol and (*b*) propanol alcohol. The curves are the theoretical dispersion relations with tabular values of the capillary lengths $\lambda_* = 1.71$ mm for (*a*) and $\lambda_* = 1.68$ mm for (*b*).

harmonics. The Fourier spectrum is now averaged over the angle to give the radial spectrum. Figures 4(*a*), 4(*b*) and 4(*c*) show, for $\omega/\pi = 380$ Hz and $f = 1.03 f_c$, the surface state, the spatial Fourier spectrum, and the radial spectrum, respectively. The radial spectrum displays a series of equidistantly separated peaks on a nearly frequency-independent background. We now read the wavenumber from the primary peak. The accuracy of this method depends on the number of wavelengths contained in the image, i.e. the largest errors are found for low frequencies where only a few wavelengths are present ($\lambda = 7.5$ mm for the forcing frequency $\omega/\pi = 50$ Hz). Figures 5(*a*) and 5(*b*) show the resulting wavelength λ as functions of drive frequency ω/π for ethanol and propanol. The solid lines are the theoretical dispersion relation (9), with the tabular values 1.71 and 1.68 mm for the capillary length λ_* at the temperature $T = 20$ °C. The agreement with theory is excellent. The measurements have been repeated for higher values of the drive amplitude, where the circular pattern is unstable. We do not find any significant change in the wavenumber.

From the nonlinear theory, the detuning σ is estimated to be $\sigma \approx \gamma(2\epsilon)^{1/2}$. For $\epsilon = 0.03$, we find $\Delta\lambda/\lambda \approx \sigma/\omega = 0.005$ in the entire frequency range studied. This estimate

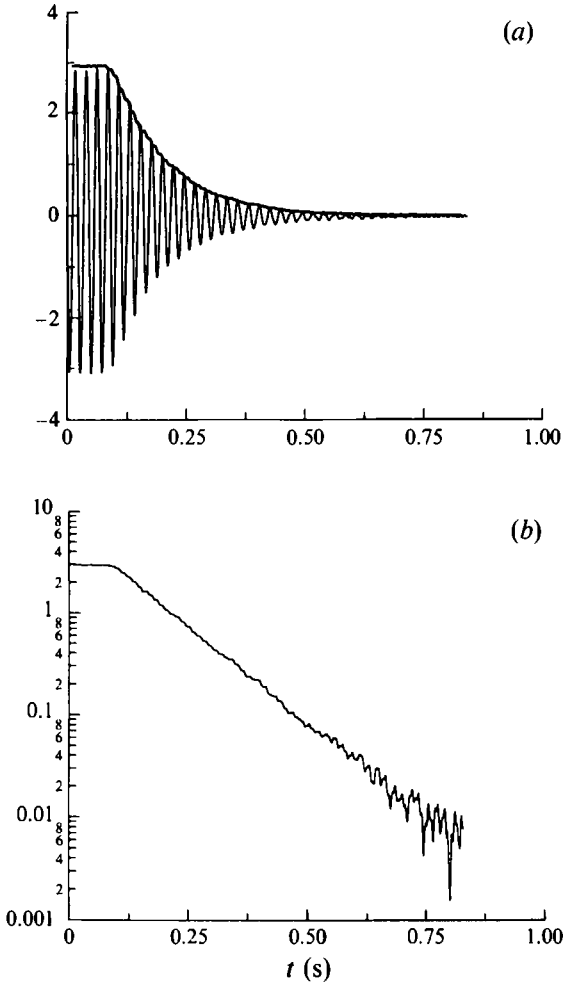

FIGURE 6. The decay of the surface wave amplitude after shutting off the exciter. (*a*) The thin curve is the signal from the photo diode. The heavy curve is the envelope obtained by complex demodulation. (*b*) The envelope in a semi-logarithmic plot.

strongly supports the excellent agreement between experiment and linear theory. For more viscous fluids a difference from linear theory should become visible.

3.3. *The damping*

We have performed direct measurements of the damping rate γ of the surface waves. Such experiments have previously been conducted only for low frequencies (Henderson 1990, 1991), where the damping is dependent on the modal structure of the wave state.

We excited the surface waves with a drive amplitude slightly above the critical f_c, in the region where the circular state is stable, as we are interested in the linear damping rate ($\epsilon \approx 0.02$). We then turned the shaker off, and recorded the time series measured with the photo diode while the wave decayed. We chose a sampling rate giving 50–200 points per period. Figure 6(*a*) shows the time series for $\omega/\pi = 88$ Hz. We note that the series is not perfectly symmetrical, a fact we attribute to the nonlinear optical process in the measurement (Christiansen 1992). To remove the basic frequencies, i.e. ω and its harmonics, we used complex demodulation of the time series (Bloomfield 1976) with

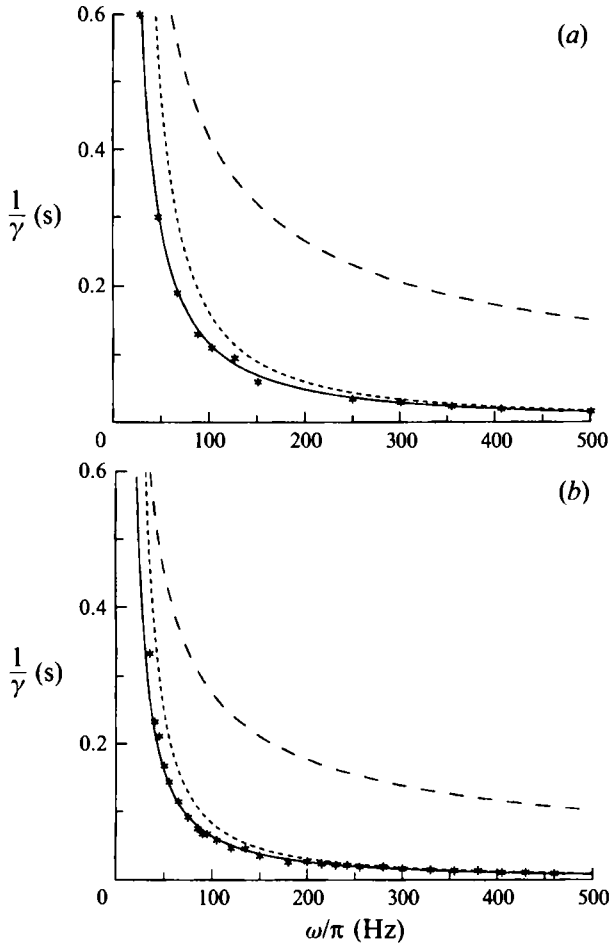

FIGURE 7. The damping rate $1/\gamma$ obtained in a cell of diameter 8.4 cm. The two dashed lines show the theoretical prediction including only bulk damping or damping from a moving contact line, respectively. The full curve shows the prediction when both are included. (*a*) Ethanol, with parameter $\nu = 1.19 \times 10^{-2}$ cm s^{-1}, $\rho = 0.8$ g cm^{-3}, $\lambda_* = 0.171$ cm, and $s = 10^{-6}$ cm. (*b*) Propanol, with parameters $\nu = 2.25 \times 10^{-2}$ cm^2 s^{-1}, $\rho = 0.8$ g cm^{-3}, $\lambda_* = 0.168$ cm, and $s = 10^{-5}$ cm.

a simple moving average filter. The result is shown with the thick curve in figure 6(*a*). The wiggles on the envelope are an artifact of the demodulation. Figure 6(*b*) shows the demodulated signal in a semi-logarithmic plot. The exponential character of the decay is evident over many periods of the underlying oscillation. The (absolute) slope in figure 6(*b*) is the damping rate.

A fundamental requirement of the above procedure is that the time for the shaker to halt is considerably less than the damping time $1/\gamma$ of the waves. This seems to be the case for the frequencies under consideration. Several runs have been done for each frequency and the error was estimated to be about 5%. The position of the diode was typically near the centre of the cell, where the circular pattern has maximum amplitude. Close to the boundary the circular pattern has no amplitude, thus limiting the experimental studies to the central region. There, different positions were tried and no discrepancy found.

The resulting damping rates for ethanol are plotted in figure 7(*a*) as function of the frequency ω/π for a cell of diameter $L = 8.4$ cm. The three curves show the theoretical

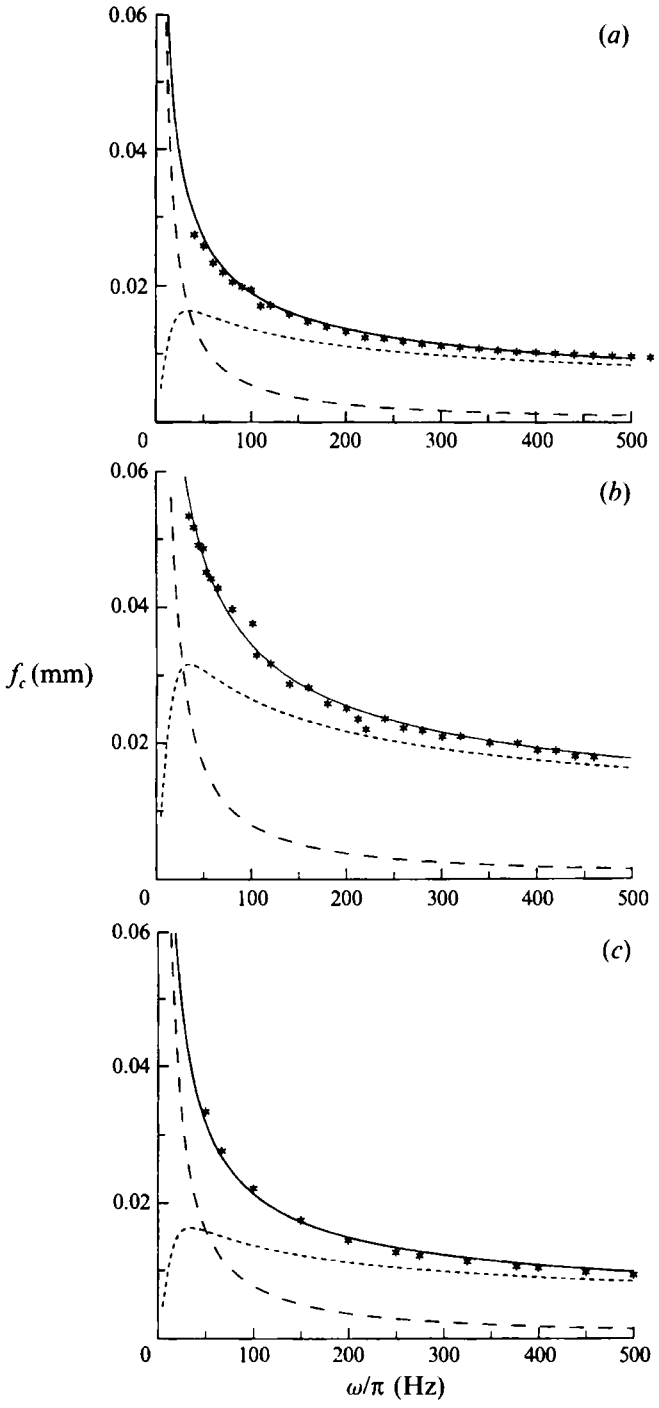

FIGURE 8. The critical amplitude f_c as a function of the drive frequency ω/π. (*a*) Ethanol: the size of the cell and the parameters are as in figure 7(*a*). (*b*) As (*a*) but in a smaller cell of diameter 5.75 cm. (*c*) Propanol: the size of the cell and the parameters are as in figure 7(*b*).

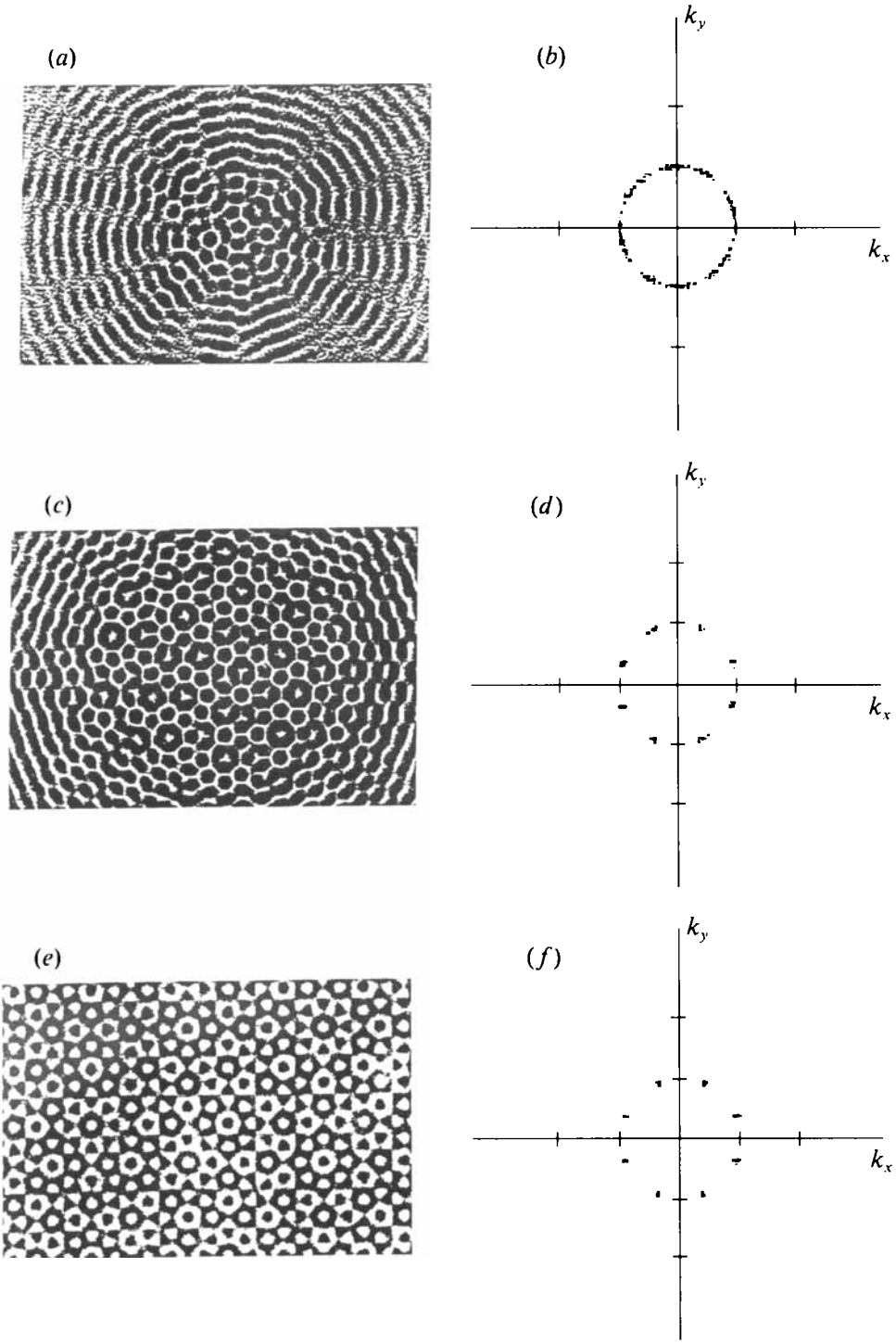

FIGURE 9. Images of capillary wave patterns (a, c) and their power spectra (b, d) obtained at a forcing frequency $\omega/\pi = 380$ Hz, and for increasing amplitudes f above f_c. The region shown is about 50% of the cell. (a, b) $f = 1.03 f_c$. (c, d) $f = 1.08 f_c$. (e, f) Computer-generated images obtained by adding four sine waves of equal amplitude.

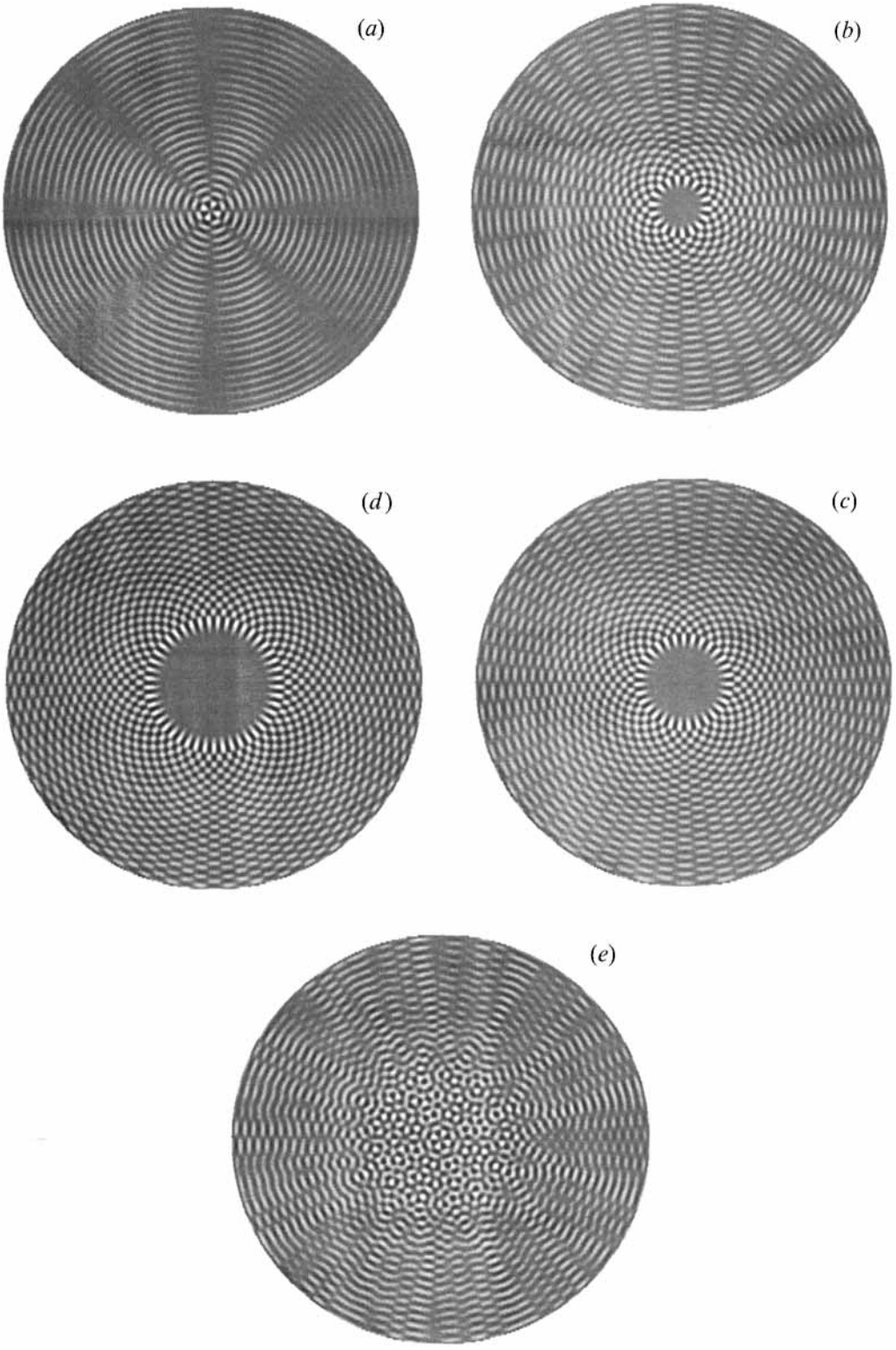

FIGURE 10. Two-dimensional plot of the normal modes $J_l(k_{lm}r)\sin(l\theta)$ for (*a*) $(l,m) = (4, 47)$; (*b*) $(l,m) = (18, 40)$; (*c*) $(l,m) = (31, 35)$; and (*d*) $(l,m) = (45, 29)$. In (*e*) the average of these modes is displayed.

values for pure bulk damping, (10), damping from the moving contact line only, (13), and for both in combination. Damping from the lateral walls is an order of magnitude less than the other contributions and has not been plotted. For the viscosity ν we have used the tabular value 0.0119 $cm^2\ s^{-1}$, and the slip length $s = 10^{-6}$ cm is chosen for the theory to fit the data. The agreement between theory and experiment is good. For high frequencies the bulk damping dominates, while damping from the moving contact line prevails for low frequencies. A characteristic of the contact-line damping is its dependence on the size of the cell. We repeated the experiment in a cell of diameter $L = 5.5$ cm. In comparison with the larger cell the damping rate has increased, but again the theory fits the experiment with the same value of s as before.

The same experiment was performed with propanol alcohol. As the viscosity $\nu = 0.0225\ cm^2\ s^{-1}$ is nearly twice the value for ethanol, higher damping rates are found. The results are shown in figure 7(*b*). To fit the experimental data a somewhat larger value of the slip length, $s = 10^{-5}$ cm, was chosen for the theory to match the data. We emphasize that the data have been fitted by theory assuming only bulk damping and damping from the moving contact line. While damping from the lateral boundaries is much less than the bulk damping, contamination of the surface could easily increase the damping by a factor of four. We attribute the fact that this is not observed, to the closed cell that hinders pollution.

From the results of §2 we can estimate the magnitude of the nonlinear damping. While the system is forced, the nonlinear damping γ_{nl} balances the linear coefficient in (18), i.e. $\gamma_{nl} = \epsilon\gamma$. Thus, the maximal ratio γ_{nl}/γ when the forcing is removed is $\epsilon \approx 0.02$.

3.4. *The critical amplitude*

As for the damping rate, no systematic experimental study of the critical amplitude Γ_c has previously been undertaken in the region of high frequencies. Although some sporadic data exist, the discussion by Milner (1991) makes it clear that the critical threshold of Faraday waves for high frequencies is still an open problem.

To find the critical amplitude we start at an amplitude well below criticality. We then successively increase the amplitude by a small amount $\delta f \sim 0.01 f_c$ until the instability is observed. Between each step we wait three minutes to allow transients to decay. The instability is detected either by monitoring the surface with the camera or with a more sensitive photo diode placed above the centre of the cell. We find the same results for both procedures in agreement with the rapid growth of the amplitude just above the threshold.

In these experiments the magnetic transducer was first placed near the centre of the cell. To test that the cell vibrates as a rigid body the transducer was moved to a position near the walls and the experiment repeated. For frequencies up to 450 Hz no difference in the critical amplitude was observed. For higher frequencies the critical amplitude was found to be slightly lower ($\sim 10\%$) than before. This indicates that for the highest frequencies a small inhomogeneity is present in the vibration.

Figure 8(*a*) shows the values of f_c obtained for ethanol in the large cell. The solid lines are the theoretical estimates assuming only bulk damping, damping from a moving contact line alone ($s = 10^{-6}$ cm as before), and both together. Again the contribution from the fixed walls is an order of magnitude lower and is not shown. The agreement is good for the entire frequency range. Figure 8(*b*) shows the critical amplitude for the cell of diameter 5.75 cm. Here fitting has been done with the same s as before. The experiment has been repeated by starting above the threshold and decreasing the amplitude stepwise. No hysteresis was found. Figure 8(*c*) shows the results for propanol alcohol and again the theory fits the data.

4. The patterns

We have previously reported the sequence of crystalline patterns observed for increasing amplitudes (Christiansen *et al.* 1992). Here we will focus on the normal modes and the transition to the quasi-crystalline state. However, for completeness we close this section with a short review of patterns observed.

When f is just above the primary instability f_c a pattern is formed which is disordered in a small portion around the centre of the cell and takes the form of modulated radial waves in the rest (figure 9*a*). The pattern is determined by circular boundary conditions, and can be explained as a superposition of the normal modes $J_l(k_{lm} r)\sin(l\theta)$.† To realize this, we recall the general form of a Bessel function $J_l(r)$ of order l. When the argument r is much larger than l, the Bessel function resembles a sine function with a slowly decreasing amplitude

$$J_l(r) \sim (2/\pi r)^{1/2}\cos(r - l\pi/2 - \pi/4).$$

Note that in this limit the wavelength no longer depends on the order l. When r is much less than l the Bessel function vanishes. In the intermediate regime $r \sim l$, where $J_l(r)$ has its extremum, the form is more complicated and depends on l. Figures 10(*a*)–10(*d*) show four (computer-generated) normal modes with $(l, m) = (4, 47)$, (18, 40), (31, 35), and (45, 29), respectively. To imitate the experimental images wave maxima are shown as bright regions and wave minima as dark regions. The modes are chosen to approximately fulfil $\mathrm{d}J_l(k_{lm} R)/\mathrm{d}r = 0$, for $R = 4.2$ cm. The superposition of the modes is shown in figure 10(*e*) and displays a disordered region for small r and a sinusoidal oscillation for large r. The resemblance with figure 9(*a*) is striking. The size of the disordered central region grows as the amplitude is increased indicating the excitation of an increasing number of normal modes. Contrary to the situation for lower frequencies it has not been possible to excite a single isolated mode; even very close to f_c the pattern displays a small disordered central region.

When the amplitude is increased to 5% above the threshold f_c a sharp transition from the normal-mode range (with patterns similar to figure 9*a*) to a qualitatively different state occurs. This surface state is shown in figure 9(*c*). The state consists of four standing plane waves with wave vectors separated by 45° as is seen from the corresponding power spectrum in figure 9(*d*). The eightfold orientational order can also be discovered by counting the number of nearest neighbours to one of the centres. This pattern lacks translational symmetry while still possessing long-range order. Thus, it forms a quasi-crystal. For comparison figures 9(*e*) and 9(*f*) show the computer-generated images produced by adding four sine waves of equal amplitudes $\sum_{j=1}^{8}\exp(\mathrm{i}\boldsymbol{k}_j\cdot\boldsymbol{x})$, with wave vectors symmetrically arranged on the circle, $\boldsymbol{k}_j = (2\pi/\lambda)(\sin(\frac{2}{8}\pi j), \cos(\frac{2}{8}\pi j))$. Many features of the experimental picture are apparent in this image. We notice however that there are also clear differences, mainly due to nonlinear optical effects, that produce higher harmonics in the experimental picture (Christiansen 1992). The quasi-crystal fills approximately the central 50% of the cell. Near the cell boundaries single lines are observed. The pattern is very stable; it persists for hours and only occasionally a defect is generated at the boundary. The quasi-crystalline pattern breaks down 9% above f_c.

For higher values of the forcing a hexagonal and a square pattern is observed. The phase diagram has previously been reported (Christiansen *et al.* 1992). The crystalline

† We acknowledge stimulating discussions with W. S. Edwards on this point.

patterns are found in a wide frequency range (340–500 Hz). At the lower cutoff frequency 340 Hz the aspect ratio is 45. If the size of the cell is decreased the cutoff frequency increases, keeping the aspect ratio constant. If the depth of the fluid is decreased to be comparable with the wavelength we observe an increase in the cutoff frequency.

In order to study boundary effects, experiments were carried out using containers with square and irregularly shaped boundaries. The previously described sequence of patterns above the normal-range was still observed, including the quasi-crystalline pattern. The shape of the boundary seems not to influence the pattern selection. However, from our discussion on the nonlinear theory we note that the pattern selection may be strongly influenced by changes in the damping rate. One may speculate whether the patterns selected are determined by a changing damping rate over several capillary lengths near the boundary.

5. Conclusions

We have measured the dispersion relation, the damping rates, and the critical thresholds for a wide range of frequencies. The experiments agree with the predictions of the linear theory if damping from the moving contact line is included in addition to the bulk damping. The value of the only free parameter s is found to be a factor 10–100 less than the value suggested by Milner (1991). The microscale s depends on the molecular structure of the fluid and the roughness of the surface of the cell. No systematic study of s has been undertaken.

The seemingly disordered state observed in a cylindrical cell immediately above the primary instability has been shown to originate from a superposition of Bessel modes. Far from the centre of the cell wavelengths are independent of the order of the Bessel modes and the boundary condition forces the individual modes to be in phase. The resulting pattern is a set of concentric circles. Near the centre of the cell, where the behaviour of the modes depends strongly on their order, the superposition gives the impression of a disordered pattern.

The first state observed above the normal-mode range is the octagonal quasi-crystalline pattern. This pattern is also observed in irregularly shaped containers. Whether this pattern is the most stable in the infinite plane at a suitable damping rate remains to be theoretically shown. So far there exists no theory that predicts which pattern is the most stable in the infinite plane at low viscosities or at high viscosities. Studies of high-aspect-ratio experiments at intermediate viscosities ($\nu k^2/\omega \approx 0.1$) would be very useful.

REFERENCES

ALEKSANDROV, V. E., BASOV, B. I., LEVIN, B. V. & SOLOV'EV, S. L. 1986 On the formation of dissipative structures at the seaquakes. *Dokl. Akad. Nauk SSSR* **289**, 1071.

BENJAMIN, T. B. & URSELL, F. 1954 The stability of the plane free surface of a liquid in vertical periodic motion. *Proc. R. Soc. Lond.* A **255**, 505.

BLOOMFIELD, P. 1976 *Fourier Analysis of Time Series: An introduction.* Wiley.

CHRISTIANSEN, B. 1992 Faraday waves and collective phenomena in coupled oscillators. Thesis, Copenhagen.

CHRISTIANSEN, B., ALSTRØM, P. & LEVINSEN, M. T. 1992 Ordered capillary-wave states: Quasicrystals, hexagons, and radial waves. *Phys. Rev. Lett.* **68**, 2157.

CILIBERTO, S. & GOLLUB, J. P. 1984 Pattern competition leads to chaos. *Phys. Rev. Lett.* **52**, 922.

CILIBERTO, S. & GOLLUB, J. P. 1985 Chaotic mode competition in parametrically forced surface waves. *J. Fluid Mech.* **158**, 381.

CROSS, M. C. & HOHENBERG, P. C. 1993 Pattern formation outside of equilibrium. *Rev. Mod. Phys.* **65**, 851.

DOUADY, S. 1990 Experimental study of the Faraday instability. *J. Fluid Mech.* **221**, 383.

DOUADY, S. & FAUVE, S. 1988 Pattern selection in Faraday instability. *Europhys. Lett.* **6**, 221.

DOUADY, S., FAUVE, S. & THUAL, C. 1989 Oscillatory phase modulation of parametrically forced surface waves. *Europhys. Lett.* **10**, 309.

EDWARDS, W. S. & FAUVE, S. 1993 Parametrically excited quasicrystalline surface waves. *Phys. Rev.* E **47**, R788.

EZERSKII, A. B., KOROTIN, P. I. & RABINOVICH, M. I. 1985 Random self-modulation of two-dimensional structures on a liquid surface during parametric excitation. *Pis'ma Zh. Eksp. Teor. Fiz.* **41**, 129 (*JETP Lett.* **41**, 157 (1985)).

EZERSKII, A. B., RABINOVICH, M. L., REUTOV, V. P. & STAROBINETS, I. M. 1986 Spatiotemporal chaos in the parametric excitation of a capillary ripple. *Zh. Eksp. Teor. Fiz.* **91**, 2070 (*Sov. Phys. JETP* **64**, 1228 (1986)).

FARADAY, M. 1831 On a peculiar class of acoustical figures, and on certain forms assumed by groups of particles upon vibrating elastic surfaces. *Phil. Trans. R. Soc. Lond.* **52**, 299.

HENDERSON, D. H. 1990 Single-mode Faraday waves in small cylinders. *J. Fluid Mech.* **213**, 95.

HENDERSON, D. H. 1991 On the damping of Faraday waves. In *Of Fluid Dynamics and Related Matters. Proc. Symp Honouring John Miles on his 70th Birthday, November 29–December 1, 1990* (ed. R. Salmon & D. Betts.) Scripps Institution of Oceanography.

JORDAN, D. W. & SMITH, P. 1977 *Nonlinear Ordinary Differential Equations*. Oxford University Press.

LAMB, H. 1963 *Hydrodynamics*, 6th edn. Cambridge University Press.

LANDAU, L. D. & LIFSHITZ, E. M. 1987 *Fluid Mechanics*, 2nd edn. Pergamon.

LEVIN, B. V. & TRUBNIKOV, B. A. 1986 'Phase transitions' in an array of parametric waves at the surface of an oscillating liquid. *Pis'ma Zh. Eksp. Teor. Fiz.* **44**, 311 (*JETP Lett.* **44**, 399 (1986)).

MALOMED, B. A., NEPOMNYASHCHII, A. A. & TRIBELSKII, M. I. 1989 Two-dimensional quasiperiodic structures in nonequilibrium systems. *Zh. Eksp. Teor. Fiz.* **96**, 684 (*Sov. Phys. JETP* **69**, 388 (1989)).

MARTIN, T. (ed.) 1932 *Faraday's Diary*. London: G. Bell.

MERON, E. & PROCACCIA, I. 1986 Low-dimensional chaos in surface waves: Theoretical analysis of an experiment. *Phys. Rev.* A **34**, 3221.

MILES, J. W. 1967 Surface-wave damping in closed basins. *Proc. R. Soc. Lond.* A **297**, 459.

MILNER, S. T. 1991 Square patterns and secondary instabilities in driven capillary waves. *J. Fluid Mech.* **225**, 81.

MÜLLER, H. W. 1993 Periodic triangular patterns in the Faraday experiment. *Phys. Rev. Lett.* **71**, 3287.

NEWELL, A. C. & WHITEHEAD, J. A. 1969 Finite bandwidth, finite amplitude convection. *J. Fluid Mech.* **38**, 279.

RAYLEIGH, LORD 1883 On the crispations of fluid resting upon a vibrating support. *Phil. Mag.* **16**, 50.